# MEASUREMENTS AND MODELING OF LOW NOx EMISSION IN NATURAL GAS / WET AIR SWIRL DIFFUSION FLAME

Sébastien Caillat, Marie-Sophie Cabot, Gilles Cabot

# MEASUREMENTS AND MODELING OF LOW NOx EMISSION IN NATURAL GAS / WET AIR SWIRL DIFFUSION FLAME

**S. CAILLAT**
Université de Rouen / CORIA UMR CNRS 6614
76134 Mont Saint Aignan Cedex, France
Tel.: 33 235 146 367 Fax: 33 235 146 371
Sebastien.Caillat@coria.fr

**M. S. CABOT**
76160 Bois L'Evêque France
Tel./fax: 33 235 021 867
Marie-Sophie.Cabot@univ-rouen.fr

**G. CABOT**
Université de Rouen, IUT, Dépt Génie Thermique
76134 Mont Saint Aignan Cedex, France
Tel.: 33 235 146 367 Fax: 33 235 146 371
Gilles.Cabot@univ-rouen.fr

## ABSTRACT

The effect of vapor water injection on the pollutant emissions is studied in laboratory natural gas burner $CH_4$ / air, based on a confined axially symmetric geometry. The swirl diffusion flame is fully turbulent.

It is first verified that the laboratory burner reproduces the trends measured on industrial systems, in terms of pollutant global emissions when water concentration is increased. The detailed study of the laboratory burner includes local measurements on profiles at different height in the flame of temperature (thin thermocouple), velocities (LDA) and chemical species ($CO_2$, CO, NO, $O_2$) concentrations (analysis system). Flame maps obtained by planar Laser Induced fluorescence of OH are performed.

Results obtained for three different values of specific humidity namely 0, 58, and 78 gram $H_2O$ per kg of dry air, are presented, and compared with results obtained by numerical simulation of the burner, using the computational fluid dynamics code Fluent.

## NOMENCLATURE

| | |
|---|---|
| BFC | Body Fitted Coordinates |
| CFD | Computational Fluid Dynamic |
| LDA | Laser Doppler Anemometry |
| LIF | Laser Induced Fluorescence |
| PAVE | Pompe à Vapeur d'Eau, Water Vapor Pump |
| RSM | Reynolds Stress Model |
| d | diameter |
| r | specific humidity, g of water per kg of dry air ($10^{-3}$ kg/kg) |
| z | axial position, relative to the end of the stabilization cone |
| ε | emissivity |

## INTRODUCTION

Water injection is often used as a way to decrease NOx emissions in industrial combustion devices like gas turbines and engines (Dryer, 1977, Payne and Seaba, 1995). Since the beginning of 90$^{th}$, water injection is also used in natural-gas boilers of some large-scale heating devices. In these configurations, the main effect of water injection can be an increase of the thermal efficiency, but a reduction of NOx emissions is also observed. This decrease is mainly due to the physical effect of dilution leading to the reduction of flame temperatures. However, a few studies (Miyauchi *et al.*, 1981) have shown that added water vapor can participate in the reaction process. The study of Miyauchi concerned a laminar premixed methane/air flame. In the present study, the configuration used is close to industrial configurations of natural-gas burners. The flame is a confined turbulent diffusion flame, stabilized by a swirl co-flow.

## EXPERIMENTAL SET-UP

### Industrial Boilers

Previous to the present study, measurements had been performed on industrial methane boilers using humid-air for combustion purposes. These plant boilers are equipped with water vapor pumps (PAVE). A schematic representation of a PAVE is presented in Fig. 1, and its physical basis is explained thereafter: Combustion air is pre-heated and humidified by exchange with combustion products. The consequence is that water in combustion products condenses at a higher temperature. That means that condensation is possible for inlet water temperature ranging to typically 90 °C whereas it is limited to typically 60 °C in classical installations. This leads to thermal efficiencies always higher than 90% on Higher Heating Value of the fuel (Guillet *et al.*, 1995). Some measurements were performed in two different installations: first, an industrial prototype 180-220 kW (Caillat, 1997) and second, an institutional heating boiler of 200-500 kW.

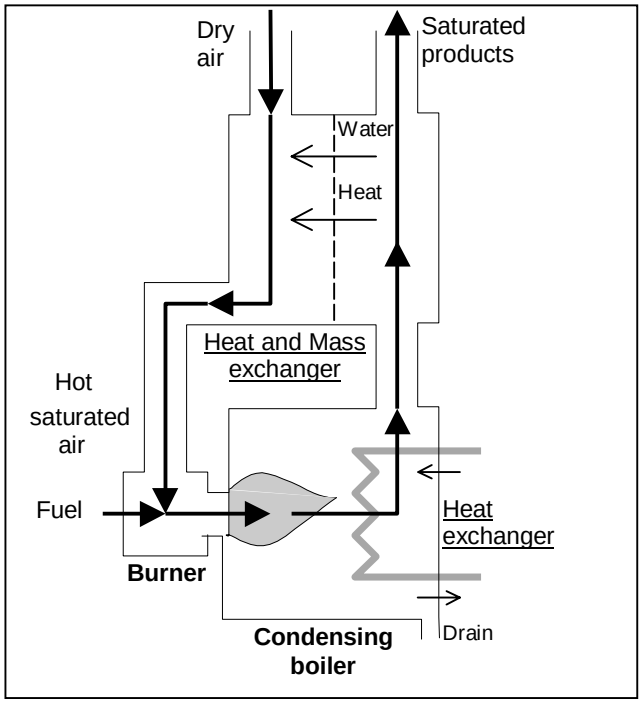


Fig.1: Boilers equipped with water vapor pump

In both cases, the specific humidity ranges from 0 to 150 g of water per kg of dry air, which is a water/fuel ratio of 3 kg/kg.

**Laboratory Burner**

A 7 kW laboratory burner, with axially symmetric geometry, and turbulent diffusion flame with swirl was developed for the present study. The burner (Fig. 2) is composed of an annular fuel injector ($d_{in}$ = 6 mm, $d_{out}$ = 8 mm) surrounded by a rotating humid air flow ($d_{in}$ = 10 mm, $d_{out}$ = 15.5 mm). The flow is confined into a stabilization cone (angle 30°, height 16 mm) then develops into the combustion chamber (d = 0.162 m, height H = 1 m). Air and methane flow-rates are measured and controlled with sonic nozzles.

The air is humidified in the following way: the air is first dried in a chemical air dryer, then heated up, and at last humidified until saturation in a bubbler. The humid air is then overheated in order to prevent condensation in the pipes. The bottom of the burner is also heated up to 80 °C in order to maintain a constant air temperature, and control injection conditions.

Three different cases are studied which correspond to three values of the specific humidity r: r = 0, r = 58, and r = 78 grams of water per kg of dry air. These cases will be referred thereafter as dry, 58 g and 78 g cases. Volumetric air and fuel flows are respectively 0.62 $m^3$/h and 7.4 $m^3$/h (standard conditions).

**Measurement Techniques**

The lower part of the chamber is equipped with four windows allowing optical access for LDA and LIF measurements, and physical access for thermocouple and aspiration probe.

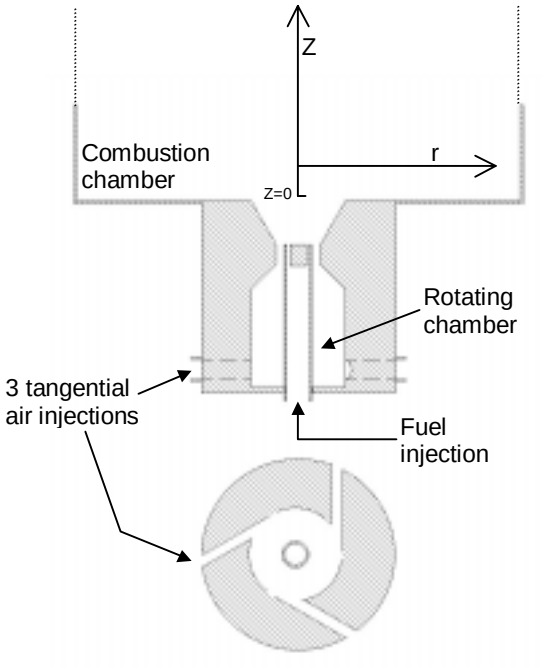


Fig. 2: Laboratory burner

Access inside the stabilization cone is not possible, and for the knowledge of boundary conditions for the calculation, additional velocity measurements were performed on the air and fuel injector without cone, and without combustion.

*Note*: the reference for axial distance (z = 0) is located at the end of the cone (Fig. 2).

**Concentration Measurements.** Concentrations of $CO_2$, CO and NO are measured by the infrared technique for, and $O_2$ with a magnetic pressure type. Local measurements are performed using a sonic expansion aspiration probe ($d_{ext}$ = 4 mm). Global measurements of pollutant concentrations are performed by sampling at the top of the combustion chamber.

**Temperature Measurements.** A thin thermocouple (d = 50 μm – platinum / platinum rhodium) is connected to a high frequency acquisition station. Local temperature measurements were performed at 5 kHz during 12 s. Mean temperatures presented in the paper includes radiation corrections for the thermocouple ($\varepsilon_{th}$ = 0.8, $\varepsilon_{wall}$ = 0.6, $T_{wall}$ = 200 °C) recommended by Neveu (1994).

**Velocity Measurements.** Instantaneous velocity measurements are performed using a two component LDA system ($\lambda_1$ = 514 nm, $\lambda_2$ = 488 nm, 350 mm focal length, 0.1×1 mm measurement volume). Air canal is seeded with 1 μm zircon powder. It was verified that the seeding in the air channel, compared with a seeding in both fuel and air channels, did not induce any measurable bias on measured velocities. This is due to fact that the central recirculation drags the powder along.

**Planar OH Laser Induced Fluorescence.** Laser Induced Fluorescence of OH is measured with a 57 mm height planar laser sheet, (sheet thickness < 1 mm, $\lambda$ = 283.5 nm, shot duration 10 ns, E = 13 mJ). The signal is recorded on a gated intensified CCD camera (576×384 pixels). Details on the LIF device can be found in Cessou and Stepowski (1996).

## Modeling Set-up

The Fluent CFD code is used, the calculation are performed on a 53×284 nodes BFC mesh (Fig. 3). Grid spacing was first optimized in the case of a cartesian mesh, by refining mesh size until stabilization of the calculated solution. The standard k-ε model is used for turbulence modeling. The following values are used for the model constants:

$$C_\mu = 0.09,\ C_{\varepsilon 1} = 1.56,\ C_{\varepsilon 2} = 1.92,$$
$$\sigma_k = 1.0,\ \sigma_\varepsilon = 1.3,\ \sigma_\Phi = 0.85$$

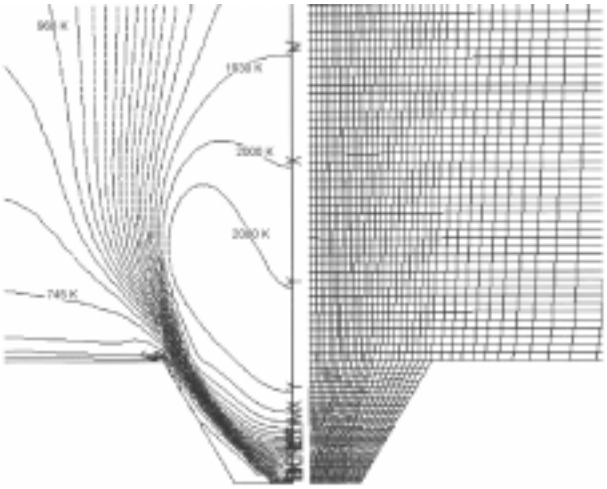

Fig. 3: Calculated temperature contour, calculation mesh (nozzle part).

The first three reactions of the five steps global mechanism of Nicol *et al.* (1998) are implemented:

$$CH_4 + \frac{3}{2}\ O_2 \rightarrow CO + 2\ H_2O \qquad (1)$$

$$CO + \frac{1}{2}\ O_2 \rightarrow CO_2 \qquad (2)$$

$$CO_2 \rightarrow CO + \frac{1}{2}\ O_2 \qquad (3)$$

The kinetic schemes of both thermal and prompt NO production will be implemented in a second step. Reader should refer to Nicol *et al.* (1998) for additional information on reaction rate constants.

Inlet boundary conditions of the calculation are reported in table 1. As above mentioned, gas velocities measurements were performed close to the nozzle (1.6 mm) in order to obtain reliable inlet conditions for the simulation.

| | Fuel | Air | | |
|---|---|---|---|---|
| | | dry | 58 g case | 78 g case |
| Inlet temperature (K) | 300 | 353 | 353 | 353 |
| Axial velocity U ($m.s^{-1}$) | 5.0 | 17.0 | 18.6 | 19.1 |
| Radial velocity V ($m.s^{-1}$) | 0 | 0 | 0 | 0 |
| Swirl velocity W ($m.s^{-1}$) | 0 | 14.0 | 15.3 | 15.7 |
| $CH_4$ mass fraction | 1 | 0 | 0 | 0 |
| $O_2$ mass fraction | 0 | 0.23 | 0.2174 | 0.2133 |
| $H_2O$ mass fraction | 0 | 0 | 0.0548 | 0.0724 |
| Turbulence | Intensity: 10 %, Length scale: 1 mm | | | |

Table 1: Inlet boundary conditions of the calculation

Injection velocities U for the humid cases were calculated from the value in the dry case $U_o$ assuming that the axial and swirl components increased linearly with the injected water vapor flow-rate:

$$U = U_o\left(1 + \frac{r \times 10^{-3}}{0.622}\right) \qquad (4)$$

Standard wall functions were applied for wall boundary conditions. A temperature of 200 °C was imposed on the lateral wall (radius 80 mm). The cone temperature and the bottom wall temperature were set to 100 °C.

The standard k-ε model, which is used here, is not recommended by authors for swirling flows. However, it leads to good results in the present configuration. R.S.M. model, which is usually recommended for non-isotropic flow, was tried but convergence problems were encountered.

## Results Obtained on Industrial Boilers – Comparison with the Laboratory Burner

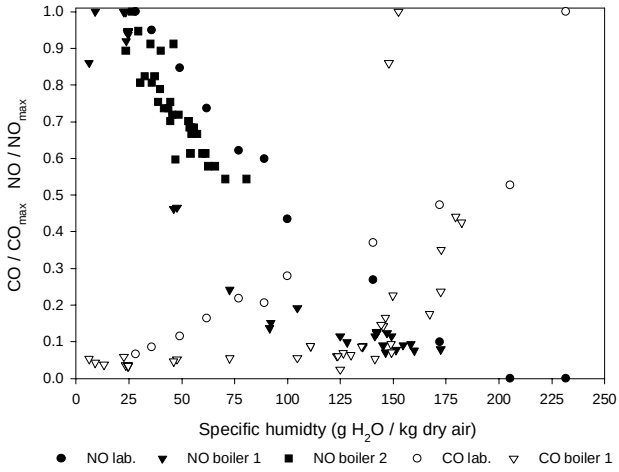


Boiler 1 (180-220 kW) $NO_{max}$ = 83 ppm $CO_{max}$ = 727 ppm
Boiler 2 (200-500 kW) $NO_{max}$ = 57 ppm CO not measured
Lab. burner (5-7 kW) $NO_{max}$ = 10 ppm $CO_{max}$ = 434 ppm

Fig. 4: NO and CO global measurements

Pollutant global emissions are presented in Fig. 4. In both industrials cases the normalized rate of NO emissions decrease severely from 1 to 0.07 when specific humidity ranges from 0 up to 150 g/kg. CO emissions remain constant up to 100 g/kg, then increase rapidly.

Laboratory burner reproduces the same trends, in terms of normalized NO and CO emissions. However, the maximum levels of NO emissions ranges from 10 ppm for the laboratory burner to 57 and 83 ppm for the two industrial devices. This is due to a scaling factor, which is classical in diffusion flames: for increasing burner power, gas injection velocities are not significantly modified but nozzle dimensions are increased, which leads to longer flames. Gas residence times in high temperature zone are increased, inducing an increase of NO production.

## RESULTS ON LABORATORY BURNER

### Flow Structure and Flame Shape

The flow structure, in the dry air case, can be noticed on the vector field of LDA measured velocities (Fig. 5). A central recirculation zone can be observed under z = 37 mm. This recirculation is due to the high swirl number (≈ 0.8) and to the presence of a bluff body at the center of the injector. In consequence hot products are re-injected in the center of the flame, this phenomena enhances flame stabilization.

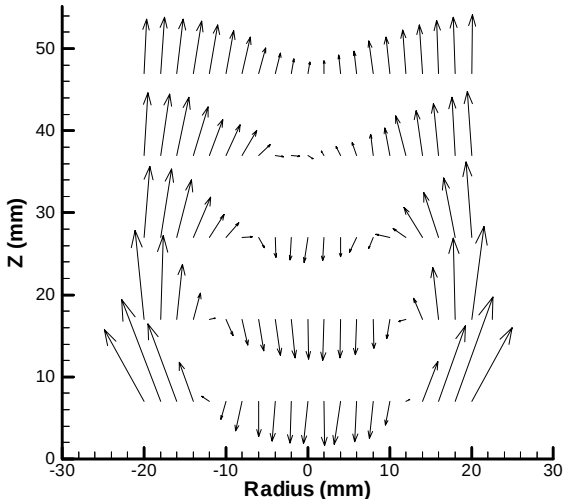


Fig. 5: Axial and radial velocity, dry case

Figure 6 presents mean and instantaneous map of OH - LIF, in the dry air case. The instantaneous map shows turbulent contours, with stretched structures. The mean map was obtained by averaging 100 instantaneous images. The top of the average flame is located at approximately z = 33 mm, which corresponds to the top of the recirculation zone previously described.

When water vapor is added to the air, the flame development zone looks shorter to the eye. From velocity and LIF measurements, the following trends for flow and flame shape are observed:

- the recirculation zone observed on velocity maps is not significantly modified.
- the intensity of OH-LIF decreases (by a factor 3 between dry and 78 g/kg cases). Nevertheless, this cannot be quantitatively interpreted: the measured signal classically depends on OH quenching, on OH concentration, and also on laser light intensity which is quenched by the additional water in our case.
- the flame top position on the OH-LIF mean maps is not significantly changed. It remains approximately at the end of the central recirculation zone.

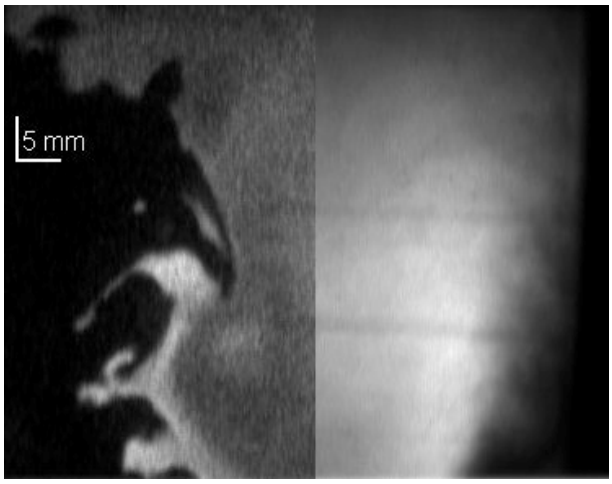


Fig. 6: Instantaneous (left) and mean (right) flame OH-LIF map, $z_{bottom}$ = 7 mm.

In numerical simulation, a recirculation core ending at z = 37 mm is also observed.

Comparisons in the non reacting case had also been performed. Experiment and simulation both lead to a central recirculation zone, which did not end inside the measured zone (z < 157 mm). Furthermore, axial velocities were predicted with about 10 % accuracy.

An excellent agreement between experimental and calculated behavior of the flame was observed. In both cases, extinction occurs when the stabilization cone is suppressed, or when water vapor concentration is increased.

Flame development is linked to the kinetic model used: the Westbrook (1984) model implementation leads to an opened flame and did not reproduce the measured behavior.

### Concentration profiles.

Local measurements of species concentration are being achieved. Only results obtained at z = 6 mm in the dry case are available, and presented in Fig. 7 with calculation results. Very good agreement can be observed on the peaks positions of CO and $CO_2$, as well as on the magnitude of these peaks.

### Velocity Profiles

Measured velocities are presented Fig 8 to Fig. 10. Figure 8 presents the velocities measured at 1.6 mm from the injector. For these measurements, it was necessary to take the cone off. Measurements were performed with no combustion, in the dry case, for fuel and air channels separately. From these profiles,

were drawn out the inlet boundary conditions of the simulation (table 1).

In figures 9 and 10, experimental velocity profiles measured at z = 7 mm and z = 47 mm are presented for the reacting dry case, and compared with the simulation results.

At z = 7 mm, axial and radial profiles are well predicted in terms of position and magnitude, but swirl velocity magnitude is slightly under-estimated by the calculation. The velocity peaks are located at the same position as the high temperature gradient zone (Fig. 12). Axial velocity reaches - 6 $m.s^{-1}$ on the axis, showing high recirculation intensity.

At z = 47 mm, good agreement between measurements and simulations is still observed for the three velocity components. Axial velocity at the center has become positive; this z position is located after the end of the recirculation, as observed previously in the velocity map.

**Temperature**

Temperature profiles are presented Fig. 11 and 12. As expected, temperature is decreased when specific humidity is increased, due to the decrease of adiabatic flame temperature with water addition (Fig.13).

Good predictions of flame width and maximum value of temperature can be observed at z = 5 mm (Fig. 11). The calculation does not predict accurately the experimentally observed minimum in the temperature profile at r = 20 mm.

At z = 43 mm (Fig. 12), the calculation under-estimate the width and over-estimate the magnitude of the temperature profile. In both figures, the temperature for radius greater than 0.03 m are correctly predicted, showing an accurate modeling of the external recirculation zone close to the lateral wall.

The flame enlargement is under-estimated while velocities are accurately predicted. This might signify that heat transfer is not correctly predicted.

Additional experimental information on reaction zone position can be found in average OH - LIF profiles at z = 8, 23, 43 mm for dry and 78 g cases (Fig. 14 to 15).

## CONCLUSION

An experimental and modeling study was initiated in order to elucidate the effect of steam addition in NO formation, for a turbulent diffusion flame. A good agreement is observed on velocity fields and on one CO / $CO_2$ profile in the lower part of the combustion chamber, in the dry air case. Still, temperatures are not well predicted in the higher part of the flame. The modeling of heat transfers inside the flame should be examined more precisely. Prior to NO calculation, it seems necessary to achieve good temperature predictions.

Additional experimental studies are now being performed:

- completion of the species measurements,
- the use of an inert gas (Argon) as dilution gas in order to suppress the effect of chemistry.

Furthermore, high sensitivity of simulation results with regard to the reduced kinetic scheme used leads us to consider more basic simulation configuration for testing purpose. The case of a laminar-premixed flame might be studied with a complete kinetic package like Chemkin and G.R.I. mechanism.

## ACKNOWLEDGEMENTS

Gaz de France is acknowledged for financial and active technical support for the present study.

## REFERENCES

Caillat, S., 1997, “Compte-rendu des mesures effectuées sur le chauffe-eau ultra-bas-NOx”, Rapport de fin de VSNE.

Cessou, A., and Stepowski, D., 1996, “Planar Laser Induced Fluorescence measurement of [OH] in the stabilization stage of a spray jet flame”, Combust. Sci. And Tech., Vol. 118, pp. 361-381.

Dryer, F. L., 1977, 16th International Symposium on Combustion, proc. pp. 279-295, The Combustion Institute.

Fluent 4.4 user’s guide, 2ND edition, May 1997.

Guillet, R., Brunel, G., Grehier, A. Viltard, J.C., 1995, “Porous Exchanger and Water Vapor Pump: the Altarex Boiler”, International Gas Research Conference, pp. 663-72.

GRI Mech. 2.11, 1995, Gas Research Institute Mechanism, on “http://www.me.berkeley.edu/gri_mech/”.

Miyauchi, T., Mori, Y., and Yamaguchi, T., 1981, “Effect of Steam Addition on NO Formation”, 18th int. Symposium on Combustion, proc. pp. 43-51, The Combustion Institute.

Neveu, F., 1994, “Mesures simultanées de la température et de la vitesse dans une flamme turbulente non prémélangée méthane - air stabilisée par un brûleur de type bluff-body”, Phd. Thesis, University of Rouen, France.

Nicol D. G. *et al.*, 1998, “Development of a 5 Step global Methane Oxidation – NO formation mechanism for lean premixed gas turbine combustion”, presented at Int. Gas Turbine & Aeroengine Cong. Stockholm - June 2-5.

Payne J. D., Seaba J. P., 1995, “Modeling the Effects of Water Vapor Addition on NO Chemistry in rich Methane - Air Flame”, 15th Int. Col. on the Dynamics of Explosions and Reactives Systems, Comb. Sci. and Techn.

Westbrook, C.K., and Dryer, F.L., 1984, Prog. In Energy and Combust. Science.

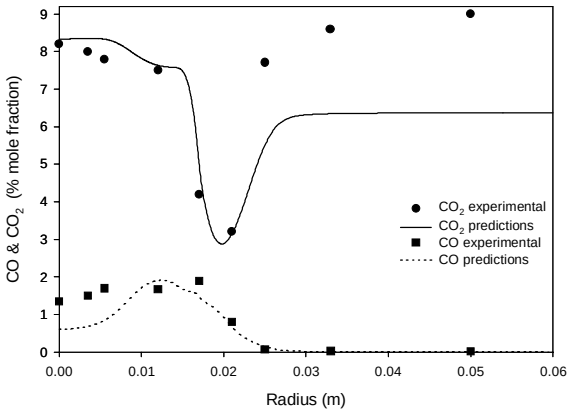


Fig. 7: CO and $CO_2$ profiles at z = 6 mm

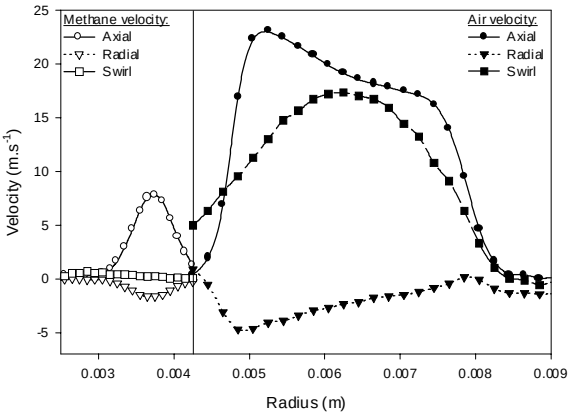


Fig. 8: Injection velocity profiles at z = 1.6 mm

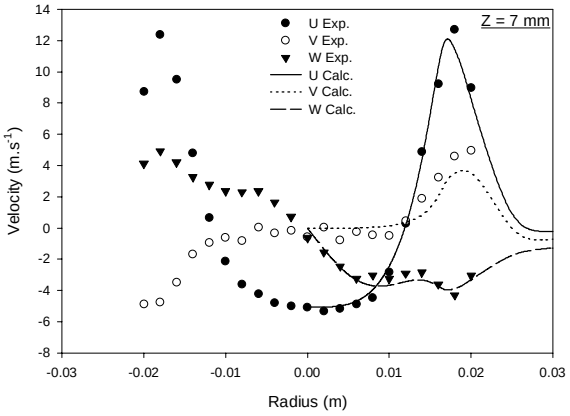


Fig. 9: Velocity profiles at z = 7 mm

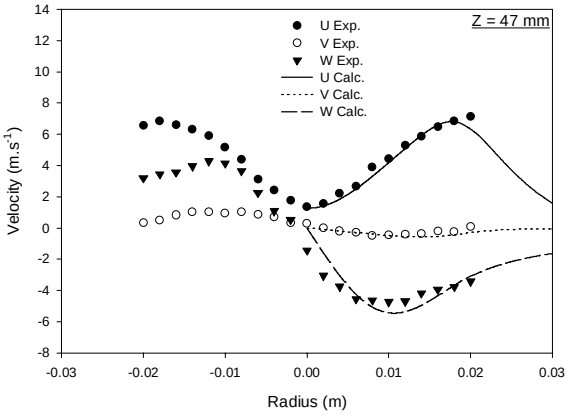


Fig. 10: Velocity profiles at z = 47 mm

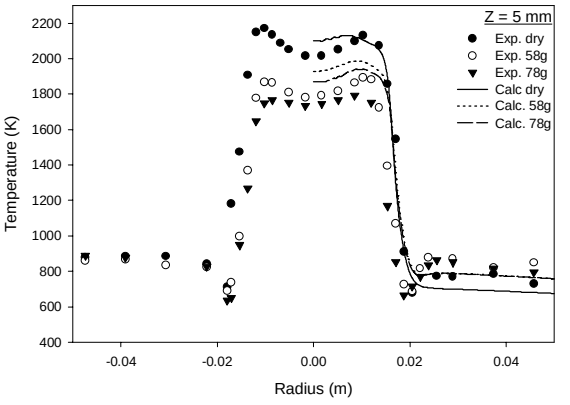


Fig. 11: Temperatures profiles z = 5 mm

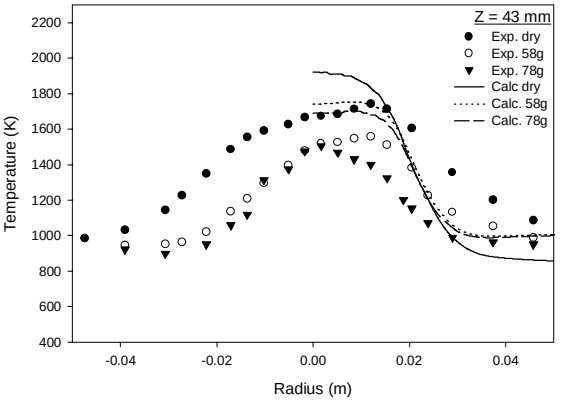


Fig. 12: Temperatures profiles z = 43 mm

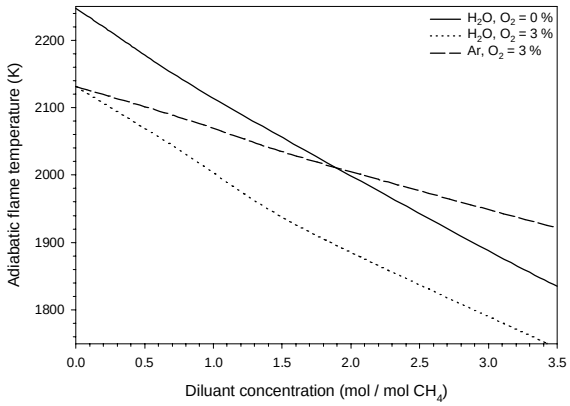


Fig. 13: Adiabatic flame temperatures calculated by Stanjan

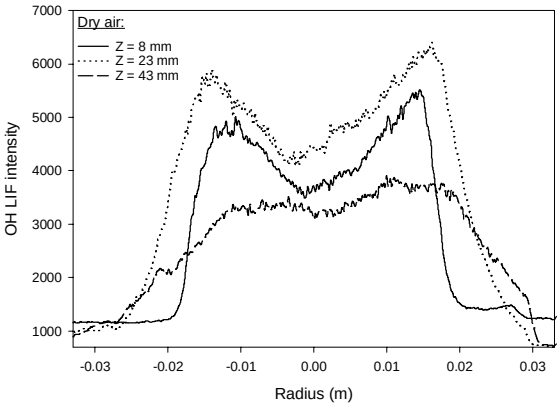


Fig. 14: OH – LIF intensity mean profiles, dry air

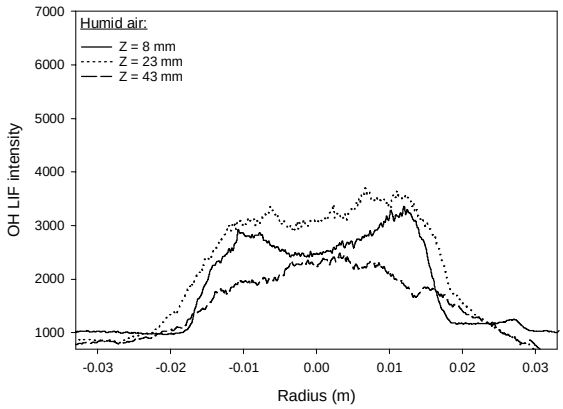


Fig. 15: OH – LIF intensity mean profiles, 78 g water air